Journal of Organometallic Chemistry, 366 (1989) 343–355
Elsevier Sequoia S.A., Lausanne – Printed in The Netherlands
JOM 09736

Molecular orbital analysis of some ligand-bridged iron binuclear complexes by UV photoelectron spectroscopy and DV-Xα calculations

M.V. Andreocci, M. Bossa, C. Cauletti

Dipartimento di Chimica, Università di Roma "La Sapienza", Piazzale A. Moro 5, Roma (Italy)

R. Paolesse, G. Ortaggi

Dipartimento di Chimica, Università di Roma "La Sapienza", Piazzale A. Moro 5, Roma (Italy) and Centro di Meccanismi di Reazione del CNR, Roma (Italy)

T. Vondrak

Dipartimento di Chimica, Università di Roma "La Sapienza", Piazzale A. Moro 5, Roma (Italy) and J. Heyrovsky Institute of Physical Chemistry and Electrochemistry, Czechoslovak Academy of Sciences (Prague)

M.N. Piancastelli

Dipartimento di Scienze e Tecnologie Chimiche, II Università di Roma "Tor Vergata", Roma (Italy)

M. Casarin

Istituto di Chimica, Università della Basilicata, via N. Sauro 85, 85100 Potenza (Italy)

M. Dal Colle and G. Granozzi

Dipartimento di Chimica Inorganica, Metallorganica ed Analitica, Università di Padova, via Loredan 4, Padova (Italy)

(Received October 21st, 1988)

Abstract

The electronic structure of $[FeCpCO]_2(\mu\text{-}CO)_2$, $[FeCpCO]_2(\mu\text{-}CO)(\mu\text{-}CH_2)$ (hereafter $Cp = \eta^5\text{-}C_5H_5$) and their methyl-substituted Cp derivatives have been accurately investigated by carrying out DV-Xα calculations and comparing the results with gas-phase UV photoelectron (PE) spectra. Some minor changes in the PE data on passing from the $(\mu\text{-}CO)_2$ to the $(\mu\text{-}CO)(\mu\text{-}CH_2)$ complexes have been interpreted in the light of the different properties of the frontier orbitals of the bridges. The reported theoretical and experimental data support the hypothesis of the lack of a direct Fe–Fe bond, in agreement with previous ab-initio theoretical results.

0022-328X/89/$03.50

Introduction

The study of the electronic structure of polynuclear organometallic complexes is of primary importance for understanding the nature of the metal–metal and metal–ligand multicentered interactions. Such information could contribute to a better understanding of the mechanism of catalytic processes once the "cluster-surface" analogy is established [1,2].

Binuclear complexes containing bridging ligands represent a particularly interesting class since the question of the existence of direct metal–metal bonding has not been clearly answered. When bridging ligands with low-lying acceptor orbitals are involved, it is not a priori clear whether the metal–metal interaction takes place via either a direct metal–metal bond or via a delocalized interaction with the bridging ligands.

In recent years there have been several gas-phase UV photoelectron spectroscopy (UV-PES) studies on bridged dimers [3]. The UV-PE data, considered along with the results of quantum-mechanical calculations, have been of value in clarifying the bonding schemes.

In the framework of our systematic investigation of the synthesis and the electronic structure of iron binuclear complexes, we present here the results of a gas-phase He-I and He-II PE study, supported by quantum mechanical calculations, on some iron μ-CO and μ-CH_2 bridged dimers of general formula:

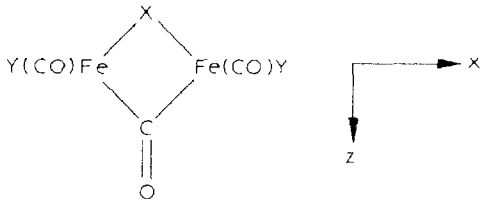

(X = CO: **1**, Y = Cp; **2**, Y = $CH_3C_5H_4$; **3**, Y = $(CH_3)_5C_5$;
X = CH_2: **4**, Y = Cp; **5**, Y = $CH_3C_5H_4$)

The He-I and He-II PE spectra of **1** have been previously discussed on the basis of ab-initio ground-state results by use of empirical rescaling constants to take account of the electronic relaxation upon ionization [4]. The lowest ionization energy (IE) band of the PE spectrum was assigned to a molecular orbital (MO) representing a four-center interaction. This MO is the highest occupied (HOMO), and originates from the mixing between an in-the-plane combination of the $2\pi^*$ orbitals of the bridging carbonyls and a π-antibonding M–M orbital. Experimental electron density [5] and theoretical data [6] are in keeping with this interpretation, since they indicate that the metal–metal interaction is not directly between the two iron atoms but acts through the bridging carbonyl groups. However, recent Fenske–Hall calculations do not agree with the ab-initio energy ordering of the highest occupied MOs, and on this basis, a different assignment for the lowest IE band of **1** was suggested [7].

The aim of this study, which extends the PE investigation to analogous molecules, is to gain a deeper insight into the character of the outermost occupied MOs. To this end, we have adopted the first-principles Discrete Variational (DV)-Xα method [8], which turns out to be particularly effective in accurately describing both

the ground state electronic structure and the energetics of the ionization process. In order to get a clearer description of the nature of the outermost MOs, correlation diagrams from the constituent fragments and MO contour plots (CPs) have also been computed.

Experimental

Preparation of 1, 2 and 3. These compounds were prepared by published methods [9]. Crude products were purified by several crystallizations from dichloromethane/hexane 1/1.

Preparation of 4. A toluene solution of calcium isopropoxyalanate (CAPAL-Assoreni) (4.8 ml, 11 mmol) was added to an anhydrous diethyl ether solution of **1** (1 g, 2.8 mmol) and the mixture was stirred for 1 h. After hydrolysis and evaporation of the organic phase, the residue was subjected to chromatography on a silicagel column. Elution with benzene/petroleum ether 1/1 produced three bands: the second one, red-violet coloured, yielded 0.7 g (71.4%) of **4** as red crystals. Its spectral data were in accord with those in the literature [10]. Separation of *cis-trans* isomers was performed by chromatography on an alumina column and elution with benzene/petroleum ether 1/1, which yielded the red-violet *trans* isomer and the red-orange *cis* isomer.

Preparation of 5. The reaction as above gave **5** (0.76 g, 67.8%) from the analogous dimer **2**.

Photoelectron spectra. The He-I and He-II gas-phase spectra were recorded on a Perkin–Elmer PS 18 spectrometer equipped with a dual He-I/He-II lamp (Helectros Development), at temperatures ranging from 110 to 200 °C. For calibration, nitrogen and self-ionizing helium were used as internal standards.

Calculations. Hartree–Fock–Slater (HFS) Discrete Variational (DV-Xα) calculations [8] of **1** and **4** were performed on a VAX 8600 (Digital Equipment Corporation) computer. The approximations involved in theoretical calculations are discussed elsewhere [8f]. Slater's transition state (TS) formalism [8g] was used to calculate the ionization energies (TSIEs). Numerical atomic orbitals (through $4p$ on Fe, $2p$ on C, O and $1s$ on H) obtained for the neutral atoms were used as basis functions. Owing to the size of the investigated systems, orbitals $1s$–$3p$ (Fe) and $1s$ on both carbon and oxygen were treated as a part of a frozen core in the molecular calculations. The MO charge density analysis was carried out by use of Mulliken's scheme [11]. The molecular geometries for **1** (C_{2h}) and **4** (C_2) were taken from the X-ray crystal structures [5,12].

Results and Discussion

Qualitative bonding schemes for the studied molecules have been extensively discussed previously [13]. The findings reported therein are used as a basis for the discussion of the DV-Xα results below.

The PE spectra of both the *cis* and *trans* isomers of each complex have been recorded, but proved to be identical. In view of the well documented rapid isomer interconversion in solution [14], the existence of a single PE spectrum in the gas-phase can be interpreted in two different ways: either there is a similar rapid

interconversion in the gas-phase (i.e. an equilibrium mixture of both isomers is obtained) or the spectrum of a single isomer is recorded and the electronic structure differences between the isomers are small. DV-Xα calculations have been carried out on both *cis* and *trans* isomers of **1** and **4**. The computed differences between their one-electron energies proved to be below the resolution of the PE technique, and this precludes a choice between the two hypotheses mentioned above. For this reason, the subsequent analysis of the PE data will be carried out only for *trans* isomers.

(μ-CO)$_2$ dimers

The spectra of complexes **1**, **2** and **3** are reported in Fig. 1. The pertinent IE values are shown in Fig. 2, in which a comparison with the DV-Xα TSIEs of **1** is shown, together with the proposed assignments. The results of ground state charge density analysis of the outermost MOs of **1** are reported in Table 1.

A useful tool to describe the bonding scheme of **1** is represented by the correlation diagram reported in Fig. 3, where the MOs of **1** are derived from interaction of the orbitals of the constituent fragments, i.e. [FeCpCO]$_2$ and (μ-CO)$_2$.

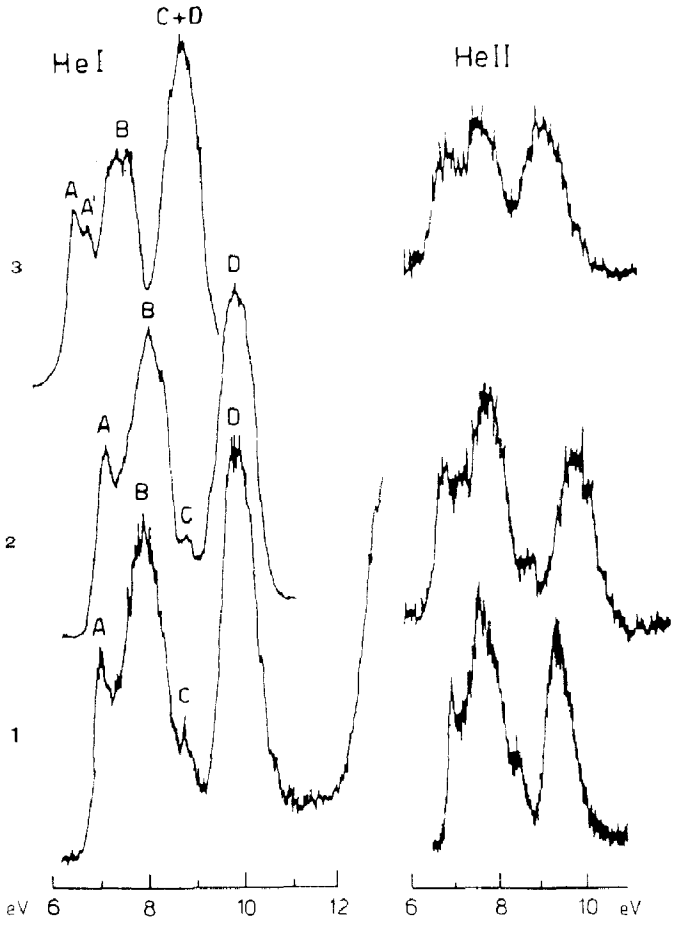

Fig. 1. He-I and He-II photoelectron spectra of **1**, **2** and **3**.

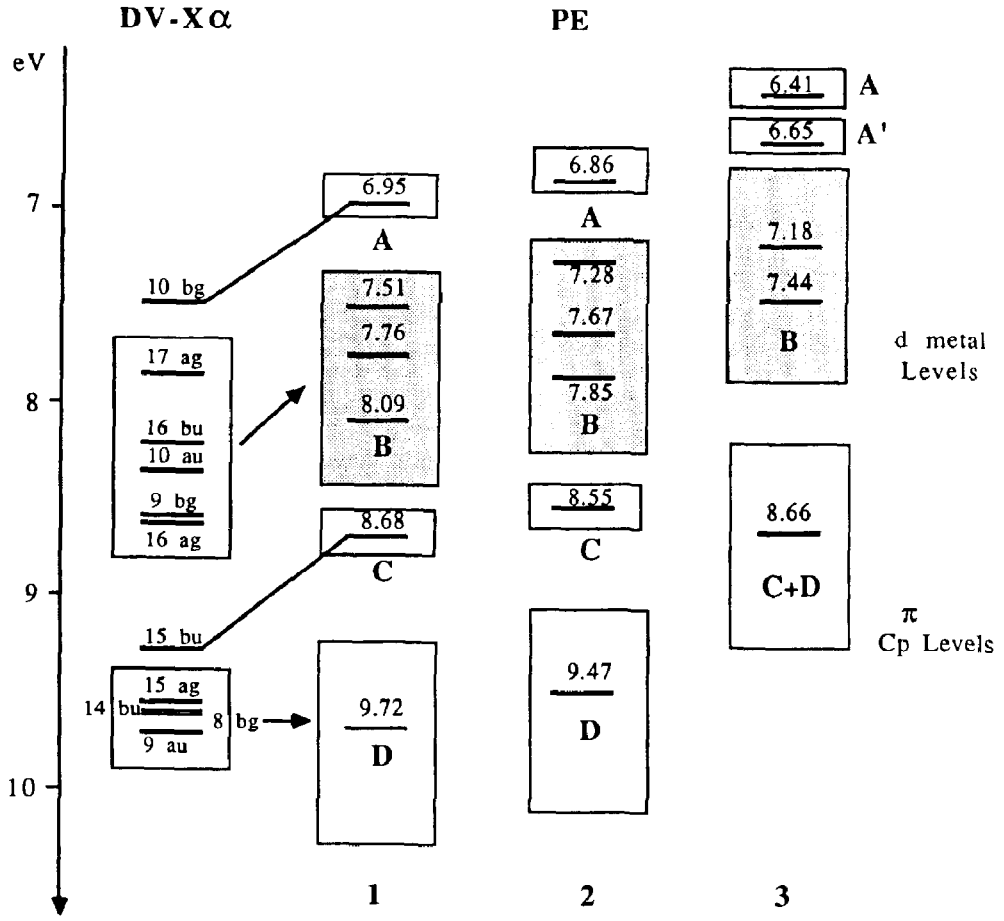

Fig. 2. Comparison between DV-Xα TSIEs of **1** and PE data of complexes **1**, **2** and **3**.

Table 1

DV-Xα results for *trans*-$[FeCpCO]_2(\mu\text{-}CO)_2$

MO	$-\epsilon$ (eV)	TSIE (eV)	Population (%)						
			2 Fe			2μ-CO	2 CO	2 Cp	Dominant character
			s	*p*	*d*				
$17b_u$(LUMO)	2.94	–	4	1	54	11	6	24	Fe–Fe $(\underline{\sigma}/\delta)^\star + \pi_+^\star \parallel$CO
$10b_g$(HOMO)	5.04	7.47	–	5	32	40	5	18	Fe–Fe $(\pi\parallel)^\star + \pi_-^\star \parallel$CO
$17a_g$	5.35	7.86	–	1	76	–	12	11	Fe–Fe $(\pi\perp)^\star$
$16b_u$	5.68	8.23	4	–	56	38	–	2	Fe–Fe $(\sigma/\underline{\delta})^\star + \pi_+^\star \parallel$CO
$10a_u$	5.89	8.36	–	4	69	1	19	7	Fe–Fe $(\delta)^\star$
$16a_g$	6.10	8.64	–	3	83	7	2	5	Fe–Fe $(\sigma/\underline{\delta})$
$9b_g$	6.11	8.60	–	–	66	16	13	5	Fe–Fe $(\delta) + \pi_-^\star \perp$CO
$15b_u$	6.80	9.27	–	4	57	21	16	2	Fe–Fe $(\pi\perp) + \pi_+^\star \perp$CO
$15a_g$	7.34	9.57	–	1	17	1	9	72	
$14b_u$	7.36	9.59	–	2	18	3	1	76	πCp +
$8b_g$	7.39	9.62	–	–	25	7	–	68	metal contribution
$9a_u$	7.49	9.72	–	2	15	2	–	81	
$13b_u$	9.36	11.58	–	–	4	42	7	47	
$7b_g$	9.59	12.08	–	–	1	63	34	2	inner σ/πCp
$12b_u$	9.71	12.05	–	–	3	39	32	26	and CO
$14a_g$	9.84	12.03	–	1	1	6	11	81	

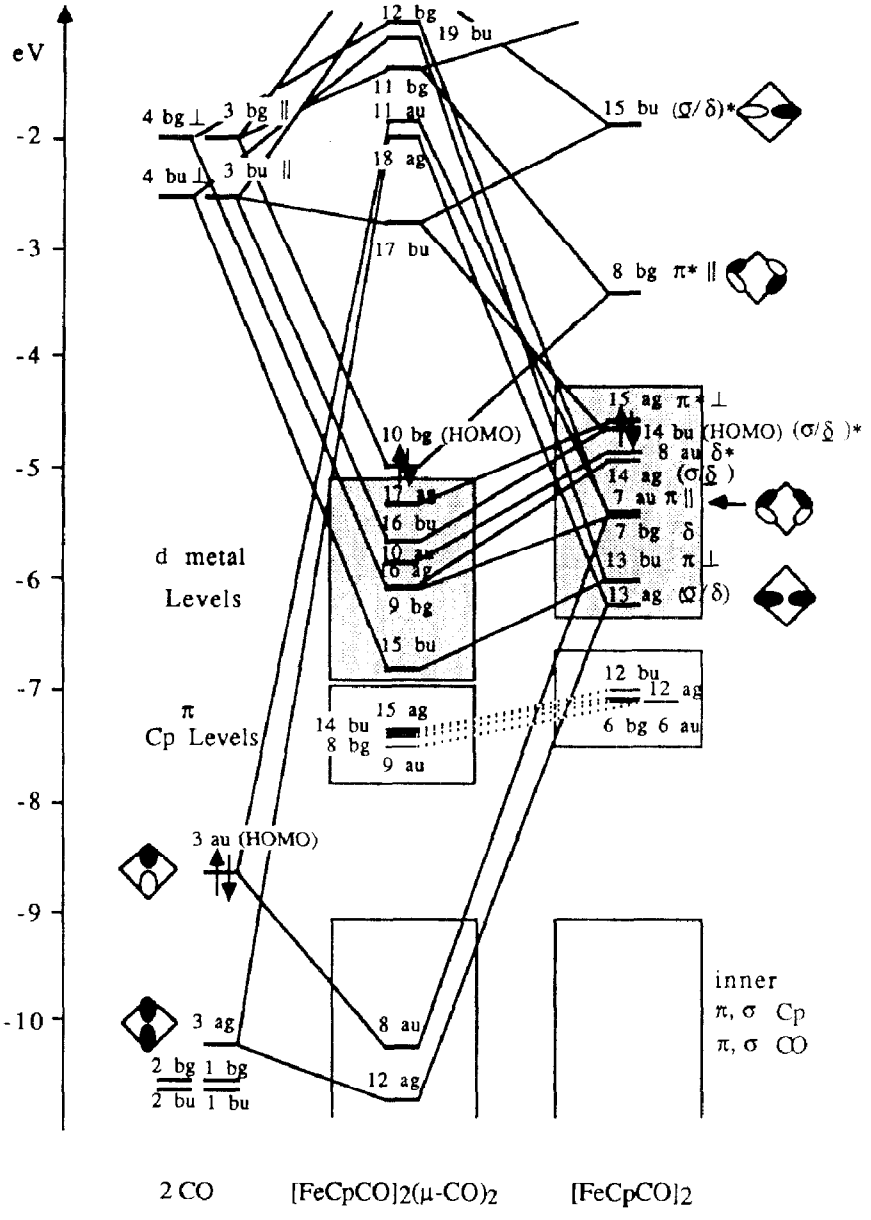

Fig. 3. DV-Xα correlation diagram of **1** starting from the constituent fragments.

nature of the MOs of the $[FeCpCO]_2$ fragment is illustrated in Fig. 3, where the symbols || and ⊥ refer to the $Fe_2(\mu\text{-}CO)_2$ plane and σ, π and δ refer to the Fe–Fe axis. Some orbitals have a mixture of σ/δ character, and the predominant one is underlined in Fig. 3 and Table 1. The outermost orbitals are metal-based MOs, referring to the pertinent Fe–Fe interactions, whereas a set of four inner orbitals are responsible for the Fe–Cp bonding. It is important to point out that the theoretical calculation on the $[FeCpCO]_2$ fragment predicts a triple bond between the two iron atoms, in keeping with the application of simple qualitative electron counting.

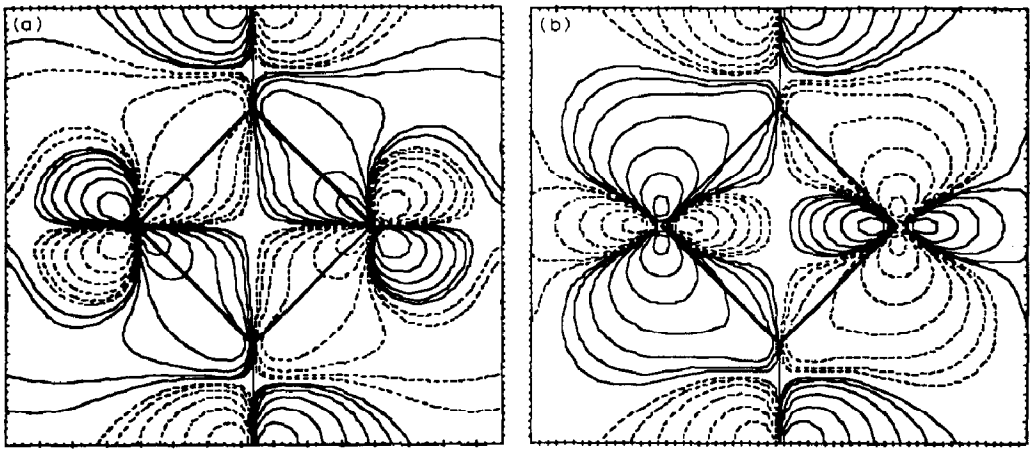

Fig. 4. DV-Xα contour plot for the (a) $10b_g$ MO and (b) $16b_u$ MOs of **1** in the plane of the $Fe_2(CO)_2$ cycle. Contour values are ± 0.0064, ± 0.0128, ± 0.0256, ± 0.0512, ± 0.1024, ± 0.2048 $e^{1/2}/Å^{3/2}$ with negative values in broken lines.

The $(\mu\text{-CO})_2$ orbitals mainly involved in the interaction with the metallic fragment are the pertinent symmetry combinations of the 5σ ($3a_g$ and $3a_u$ in Fig. 3) and $2\pi^\star$ carbonyl MOs:

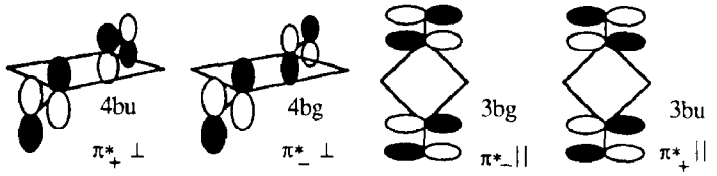

The origin of the $10b_g$ HOMO is clearly illustrated in Fig. 3 and 4a: it arises from the interaction between a $\pi^\star$ Fe–Fe orbital ($8b_g \parallel$) and the $3b_g \parallel$ combination of the $2\pi^\star$ carbonyl MOs. It nicely describes a four-center delocalized interaction, representing a concerted back-donation to the empty bridging carbonyl levels. This HOMO is well separated in energy from the subsequent set of orbitals and its ionization gives rise to the lowest IE band (labelled A in Fig. 1) of the PE spectrum, in agreement with the previous assignment proposed on the basis of ab-initio calculations [4]. In contrast, the results obtained by the Fenske–Hall method [7] predict a different HOMO, with a $\pi^\star(\perp)$ Fe–Fe nature.

The inner six orbitals (from $17a_g$ to $15b_u$) are metal-based MOs ($3d$ participation larger than 50%): the three outermost ($17a_g$ $(\pi\perp)^\star$, $16b_u$ $(\sigma/\underline{\delta})^\star$ and $10a_u$ $(\delta)^\star$) have an antibonding Fe–Fe character whereas the inner ones ($16a_g$ $(\sigma/\underline{\delta})$, $9b_g$ (δ) and $15b_u$ $(\pi\perp)$) are Fe–Fe bonding (Table 2). Among them, those of b_u and b_g symmetry show significant participation by the bridging carbonyls due to mixing with the corresponding $2\pi^\star$ orbitals. This mixing accounts, in particular, for the evident stabilization of the $15b_u$ MO, which represents a $\pi\perp$ system delocalized over the dimetallacycle (see Fig. 5), similar to that described for the analogous $[NiCp]_2(\mu\text{-CO})_2$ complex [15]. Similarly, the $16b_u$ MO represents an in-plane back-donation arising from the mixing between (M–M $(\sigma/\underline{\delta})^\star$ and $\pi^\star_+ \parallel$ CO orbitals (see Fig. 4b).

Table 2

DV-Xα results for *trans*-[FeCpCo]$_2$(μ-CO)(μ-CH$_2$)

MO	$-\epsilon$ (eV)	TSIE (eV)	Population (%)							
			2 Fe			μ-CO	μ-CH$_2$	2 CO	2 Cp	Dominant character
			s	*p*	*d*					
26*b*(LUMO)	2.81	–	1	1	58	6	6	3	25	Fe–Fe (σ/δ)* + $\pi^\star_\perp$ ‖CO + *p*-CH$_2$
25*b*(HOMO)	5.12	7.65	1	5	42	35	4	4	9	Fe–Fe ($\pi\|$)* + $\pi^\star$ ‖CO
26*a*	5.14	7.63	–	2	76	–	–	11	11	Fe–Fe ($\pi\perp$)*
25*a*	5.48	7.91	1	4	70	–	–	11	9	Fe–Fe (σ/δ, $\delta^\star$)
24*b*	5.60	8.07	–	1	71	6	6	11	5	Fe–Fe (δ)
24*a*	5.79	8.30	1	2	78	3	2	9	5	Fe–Fe (σ/δ, $\delta^\star$)
23*b*	6.38	8.81	1	3	58	15	4	14	5	Fe–Fe($\pi\perp$) + $\pi^\star$ + $\perp$ CO
22*b*	7.04	9.31	–	–	44	1	18	–	37	Fe–Fe ($\pi\|$)* + *p*-CH$_2$
23*a*	7.11	9.30	–	2	16	1	4	6	77	π-Cp + metal contribution
21*b*	7.24	9.45	–	1	19	3	1	2	74	
22*a*	7.26	9.46	–	2	15	1	–	5	77	
20*b*	7.39	9.89	–	1	19	4	–	1	75	
21*a*	9.27	11.70	–	2	25	12	49	1	11	σ-CH$_2$ + Fe–Fe ($\pi\|$)
19*b*	9.38	11.61	–	–	4	41	4	15	36	inner σ/π-Cp and CO
18*b*	9.57	12.03	–	–	1	32	4	34	29	

These theoretical expectations find a counterpart in the PE data. Thus the broad band B, with features at 7.51, 7.76 and 8.09 eV, and its higher IE shoulder C (8.68 eV), arise from the ionizations of these *d*-based orbitals (Fig. 2). This agrees well with the observed increase in the intensity of bands B and C relative to band D on passing from the He-I to the He-II spectra [16]. Band C suffers an intensity increase smaller than that of band B because of the large participation of carbonyl ligand based atomic orbitals in the 15b_u MO.

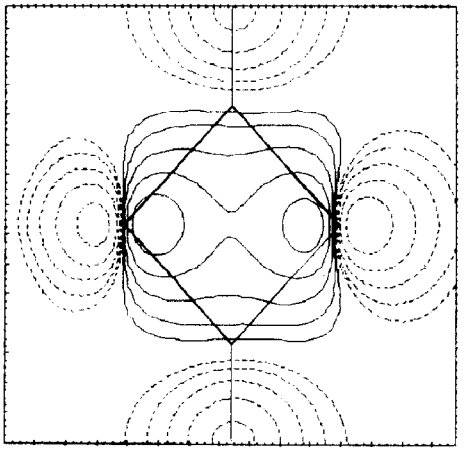

Fig. 5. DV-Xα contour plot for the 15b_u of **1** in a plane parallel (1 a.u. above) to the $Fe_2(CO)_2$ cycle. Contour values are ± 0.0064, ± 0.0128, ± 0.0256, ± 0.0512, ± 0.1024 $e^{1/2}/Å^{3/2}$ with negative values in broken lines.

The Fe–Cp bonding levels of the $[FeCpCO]_2$ fragment are virtually unperturbed by the interaction with the bridges (Fig. 3), and they maintain their character in the whole molecule. The ionization of the resulting $15a_g$, $14b_u$, $8b_g$ and $9a_u$ MOs, having a Cp character of $> 65\%$, gives rise to the intense band D, which consequently suffers a marked intensity fall-off under He-II radiation.

The substitution of a hydrogen by a methyl group in each Cp causes a shift of all bands to lower IE in the spectrum of **2** (see Fig. 2), the shift being more pronounced for band D, in agreement with its assignment to ionization of MOs with predominant Cp character. As a whole, however, the PE spectrum of **2** is very similar to that of **1**. In contrast, the spectrum of the $(CH_3)_5Cp$ analogue **3** is significantly different (see Fig. 1 and 2), showing two single bands (A, A′) at lower IE than the more intense B and C + D bands. Again the most affected ionization is that giving rise to band C + D, shifted by $\cong 0.8$ eV to lower IE with respect to that for the unsubstituted molecule (Fig. 2). This shift probably causes the disappearance, in the spectrum of **3**, of band C, which is hidden under the more intense band C + D. The new band A′ suggests that in the set of metal *d*-based MOs there is one level with higher contribution from Cp orbitals, which consequently undergoes a larger shift toward lower IE. As is evident from Fig. 2, the SHOMO (Second Highest Occupied Molecular Orbital) $17a_g$ of **1** is well separated in energy from the subsequent metal-based MOs; moreover, as reported in Table 1, this orbital presents, among those assigned to band B, the largest Cp contribution. Consequently, it seems reasonable to assign band A′ of **3** to the ionization from an orbital related to the $17a_g$ of **1**.

$(\mu$-CO)$(\mu - CH_2)$ dimers

The spectra of complexes **4** and **5** are presented in Fig. 6. They are compared with the theoretical TSIEs of **4** in Fig. 7. The fragment analysis of 4 is reported in

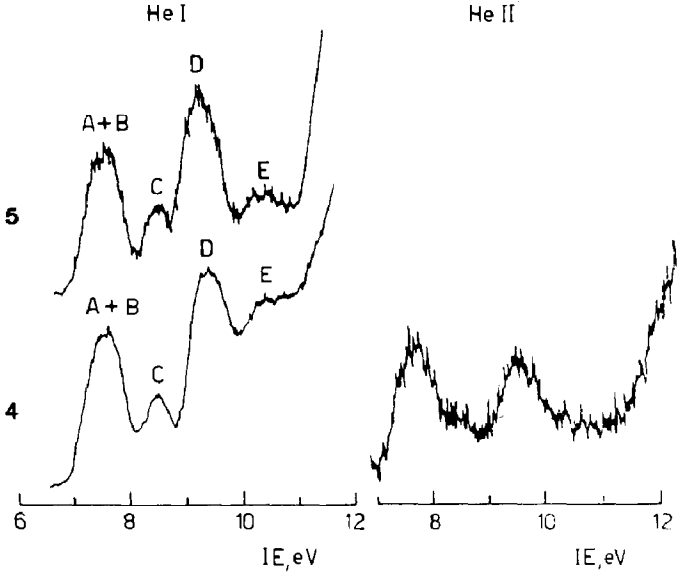

Fig. 6. He-I and He-II photoelectron spectra of **4** and **5**.

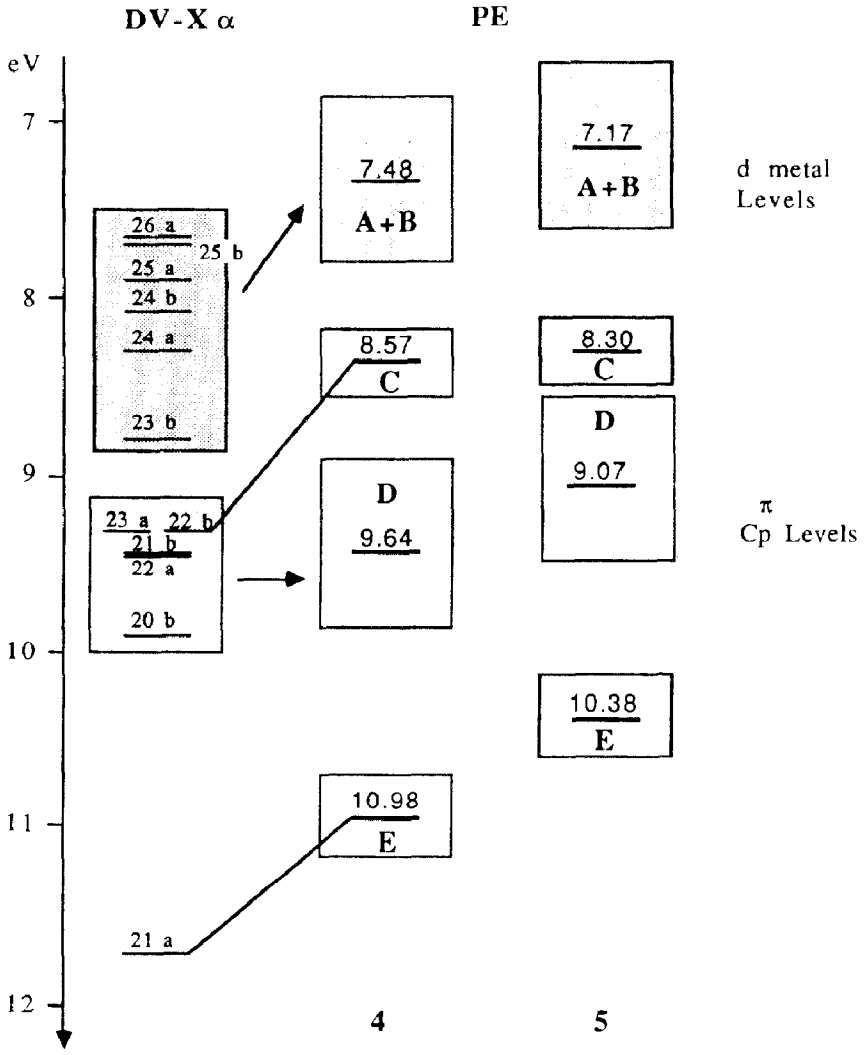

Fig. 7. Comparison between DV-Xα TSIEs of **4** and PE data of complexes **4** and **5**.

Fig. 8, while the ground state charge density of the outermost MOs is reported in Table 2.

The bonding scheme of **4** should not be too different from that of its dicarbonyl analogue. Actually, the orbitals of a bridging methylene are similar to those of a bridging carbonyl. The occupied σ lone pair is oriented in the same direction as the carbonyl 5σ MO, but lies at higher energy (compare Fig. 3 and 8). As for the vacant levels, the methylene group has only one $2p$ $\|$ orbital corresponding to the carbonyl $2\pi^*$ $\|$ one. The counterpart of the carbonyl $2\pi^*$ $\perp$ is represented by the pseudo-π C–H antibonding level, too high in energy to interact significantly. The lack of one acceptor orbital, however, is counterbalanced by the lower energy of the $2p$ $\|$ orbital (see Fig. 8), so that CH_2 as a whole is usually recorded as a better π-acceptor and σ-donor group than CO.

Difficulties, however, are encountered in the attempt to obtain an unambiguous description of the bonding of **4**, such as that obtained for **1**, because of the lower

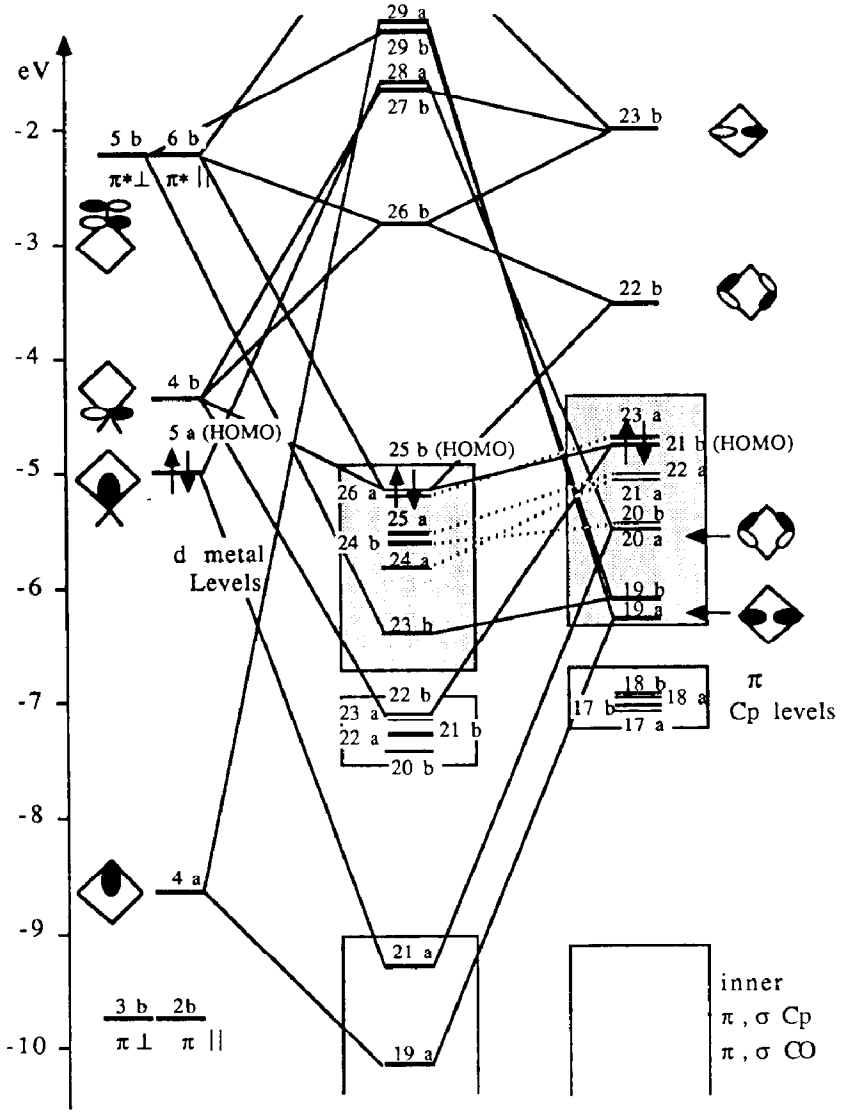

Fig. 8. DV-Xα correlation diagram of **4** starting from the constituent fragments.

molecular symmetry (C_2 vs. C_{2h}). Actually, in C_2 symmetry the MOs of the $[FeCpCO]_2$ fragment no longer have pure Fe–Fe σ, π and δ character. Moreover, the interaction with the bridges does not conform to rigid symmetry restrictions, so that it is very difficult to relate the MOs of the whole molecule to those of the fragments. For this reason the correlation diagram of Fig. 8 is less clearly interpretable, even though some major effects can be seen by comparison with the corresponding diagram of **1**. In particular, the HOMO, which was well distinct in energy from the inner orbitals in the case of **1**, in **4** appears to be more stabilized, and close in energy to the inner MOs. This is a consequence of the better energy matching between the 22*b* orbital of $[FeCpCO]_2$ with the 4*b* and 5*b* orbitals of (μ-CO)(μ-CH_2)

(μ-CO)(μ-CH_2) (Fig. 8). This theoretical expectation finds a direct counterpart in the PE spectrum (Fig. 6 and 7), where there is no distinct band to be assigned to the ionization from the HOMO, in contrast to the situation for complex **1**.

The low energy of the 4*b* level of CH_2 also accounts for the stabilization of the metal *d*-based orbital 22*b* (see Fig. 8 and Table 2), which now lies in the region peculiar to the Fe–Cp interactions. Another difference with respect to **1** is that the 23*b* MO, corresponding to the π $\perp$ delocalized $15b_u$ MO of **1** now lies at higher energy because of the absence of a π $\perp$ acceptor orbital in the CH_2 bridge.

The discussion above leads us to propose the spectral assignments reported in Fig. 7. There is no uncertainty in relating the PE band labelled as A + B (Fig. 6) to the ionizations from metal *d*-based MOs. Some problems arise in the assignment of band C, which could, in principle, be related to the ionization from 22*b* or 23*b* MOs. By analogy with the assignment for **1**, it would be tempting to assign band C to the 23*b* MO, i.e. the π $\perp$ delocalized back-donation, but according to the theoretical calculations the computed TSIE of 23*b* is ca. 0.5 eV lower than the corresponding value of the $15b_u$ MO of **1** (see Tables 1 and 2) as a consequence of the absence of a π $\perp$ acceptor orbital on CH_2. This suggests that the ionization from the 23*b* must be hidden under the broad band A + B. A more consistent assignment of band C, in keeping also with previous data on the $[MnCp(CO)_2]_2$(μ-CH_2) dimer [17], is obtained by relating this band to the ionization from the 22*b* MO, to which the $2p \parallel CH_2$ orbital contributes significantly. As usual, band D is related to MOs with Fe–Cp bonding character. The last ionization event worthy of discussion is that from the σ lone pair localized on CH_2 (21*a* MO in Table 2), which significantly contributes to the bonding within the dimetallacycle (see Fig. 8 and Table 2). This ionization probably contributes to band E, which lies at an IE similar to that for an analogous band of the PE spectrum of the mentioned (μ-CH_2) manganese dimer [17].

The PE spectrum of **5** (Fig. 6 and 7) is very similar to that of **4**, the only difference being the expected shift of all the bands to lower IE.

Conclusions

The DV-Xα theoretical data obtained have been of value in discussing and assigning the PE data of the studied bridged iron dimers. Some minor changes in the PE data found on passing from the (μ-CO)$_2$ to the (μ-CO)(μ-CH_2) complexes have been interpreted in terms of the different properties of the frontier orbitals of the bridges. In particular, the present study has demonstrated that the low-lying $2p \parallel CH_2$ empty orbital interacts more effectively with the metal atoms than the analogous CO orbital, giving rise to a stable Fe $\rightarrow$ $CH_2 \parallel$ back-donation orbital. On the other hand, the absence of a CH_2 acceptor orbital perpendicular to the dimetallacycle disfavours stable delocalized Fe $\rightarrow$ bridge $\perp$ back-donation, in contrast to the situation with the (μ-CO)$_2$ system.

Acknowledgement

Financial support for this study from Ministero della Pubblica Istruzione (Roma) is gratefully acknowledged.

Notes and references

1 R. Ugo, Catal. Rev., 11 (1975) 225.
2 E.L. Muetterties, T.N. Rhodin, E. Band, C.F. Brucker and W.R. Pretzer, Chem. Rev., 79 (1979) 91.
3 G. Granozzi, Invited lecture at EUCMOS XVIII, Amsterdam 1987, J. Mol. Struct., 173 (1988) 313 and ref. therein.
4 G. Granozzi, E. Tondello, M. Bénard and I. Fragalà, J. Organomet. Chem., 194 (1980) 83.
5 A. Mitscher, B. Rees and M.S. Lehmann, J. Am. Chem. Soc., 100 (1978) 3390.
6 M. Bénard, Inorg. Chem., 18 (1979) 2782.
7 B.E. Bursten and Cayton R.H., J. Am. Chem. Soc., 108 (1986) 8241.
8 (a) F.W. Averill and D.E. Ellis, J. Chem. Phys., 59 (1973) 6411; (b) A. Rosen, D.E. Ellis, H. Adachi and F.W. Averill, J. Chem. Phys., 65 (1976) 3629 and ref. therein; (c) W.C. Trogler, D.E. Ellis and J. Berkowitz, J. Am. Chem. Soc., 101 (1979) 5896; (d) W. Kohn and L.J. Sham, Phys. Rev. A, 140 (1965) 1133; (e) R. Gaspar, Acta Phys. Acad. Sci. Hung., 3 (1954) 263; (f) M. Casarin, D. Ajò, A. Vittadini, D.E. Ellis, G. Granozzi, R. Bertoncello and D. Osella, Inorg. Chem., 26 (1987) 2041; (g) J.C. Slater, in Quantum Theory of Molecules and Solids. The Self-Consistent Field For Molecules and Solids, vol. 4, McGraw-Hill, New York, 1974.
9 (a) R.B. King, In Organometallic Synthesis, vol. I, Academic Press, New York; (b) R.B. King and A. Efraty, J. Am. Chem. Soc., 93 (1971) 4950.
10 C.P. Casey, P.J. Fagan and W.H. Miles, J. Am. Chem. Soc., 104 (1982) 1134.
11 R.S. Mulliken, J. Chem. Phys. 23 (1955) 1833.
12 R. Korswagen, R. Alt, D. Speth and M.L. Ziegler, Angew. Chem. Int. Ed. Engl., 20 (1981) 1049 and private communication.
13 E.D. Jemmis, A.R. Pinhas and R. Hoffmann, J. Am. Chem. Soc., 102 (1980) 2576.
14 (a) F.A. Cotton and G. Yagupsky, Inorg. Chem., 6 (1967) 15; (b) A.R. Manning, J. Chem. Soc., A, (1968) 1319; (c) M.I. Altbach, C.A. Muedas, P. Korswagen and M.L. Ziegler, J. Organomet. Chem., 306 (1986) 375.
15 G. Granozzi, M. Casarin, D. Ajò and D. Osella, J. Chem. Soc. Dalton Trans., (1982) 2047.
16 (a) U. Gelius, in D.A. Shirley (Ed.), Electron Spectroscopy; North Holland, Amsterdam, 1972, p. 311; (b) J.W. Rabalais in Principles of UV Photoelectron Spectroscopy, Wiley Interscience, New York, 1977.
17 G. Granozzi, E. Tondello, M. Casarin, D. Ajò, Inorg. Chim. Acta, 48 (1981) 73.